6-26-2019

Magnetic structure and magnetization of z -axis helical Heisenberg antiferromagnets with XY anisotropy in high magnetic fields transverse to the helix axis at zero temperature

David C. Johnston
Iowa State University and Ames Laboratory, dcj99@ameslab.gov

Magnetic structure and magnetization of z -axis helical Heisenberg antiferromagnets with XY anisotropy in high magnetic fields transverse to the helix axis at zero temperature

Abstract
A helix has a wave vector along the z axis with the magnetic moments ferromagnetically aligned within xy planes with a turn angle kd between the moments in adjacent planes in transverse field H=Hxˆi=0. The magnetic structure and x-axis average magnetization per spin of this system in a classical XY anisotropy field HA is studied versus kd, HA, and large Hx at zero temperature. For values of HA below a kd-dependent maximum value, the xy helix phase transitions with increasing Hx into a spin-flop (SF) phase where the ordered moments have x, y, and z components. The moments in the SF phase are taken to be distributed on either one or two xyz spherical ellipses. The minor axes of the ellipses are oriented along the z axis and the major axes along the y axis where the ellipses are flattened along the z axis due to the presence of the XY anisotropy. From energy minimization of the SF spherical ellipse parameters for given values of kd, HA, and Hx, four kd-dependent SF phases are found: either one or two xyz spherical ellipses and either one or two xy fans, in addition to the xy helix/fan phase and the paramagnetic (PM) phase with all moments aligned along H. The PM phase occurs via second-order transitions from the xy fan and SF phases with increasing Hx. Phase diagrams in the Hx–HA plane are constructed by energy minimization with respect to the SF phases, the xy helix/fan phase, and the xy SF fan phase for five kd values. One of these five phase diagrams is compared with the magnetic properties found experimentally for the model helical Heisenberg antiferromagnet EuCo2P2 and semiquantitative agreement is found.

Disciplines
Condensed Matter Physics

Magnetic structure and magnetization of z-axis helical Heisenberg antiferromagnets with XY anisotropy in high magnetic fields transverse to the helix axis at zero temperature

David C. Johnston

Ames Laboratory and Department of Physics and Astronomy, Iowa State University, Ames, Iowa 50011, USA

(Received 17 November 2018; revised manuscript received 9 May 2019; published 26 June 2019)

A helix has a wave vector along the z axis with the magnetic moments ferromagnetically aligned within xy planes with a turn angle kd between the moments in adjacent planes in transverse field $\mathbf{H} = H_x\hat{\mathbf{i}} = 0$. The magnetic structure and x-axis average magnetization per spin of this system in a classical XY anisotropy field H_A is studied versus kd, H_A, and large H_x at zero temperature. For values of H_A below a kd-dependent maximum value, the xy helix phase transitions with increasing H_x into a spin-flop (SF) phase where the ordered moments have x, y, and z components. The moments in the SF phase are taken to be distributed on either one or two xyz spherical ellipses. The minor axes of the ellipses are oriented along the z axis and the major axes along the y axis where the ellipses are flattened along the z axis due to the presence of the XY anisotropy. From energy minimization of the SF spherical ellipse parameters for given values of kd, H_A, and H_x, four kd-dependent SF phases are found: either one or two xyz spherical ellipses and either one or two xy fans, in addition to the xy helix/fan phase and the paramagnetic (PM) phase with all moments aligned along $\mathbf{H}$. The PM phase occurs via second-order transitions from the xy fan and SF phases with increasing H_x. Phase diagrams in the H_x-H_A plane are constructed by energy minimization with respect to the SF phases, the xy helix/fan phase, and the xy SF fan phase for five kd values. One of these five phase diagrams is compared with the magnetic properties found experimentally for the model helical Heisenberg antiferromagnet $EuCo_2P_2$ and semiquantitative agreement is found.

DOI: 10.1103/PhysRevB.99.214438

I. INTRODUCTION

A reformulation of the Weiss molecular field theory for Heisenberg magnets containing identical crystallographically-equivalent spins was developed recently, termed the unified molecular field theory (MFT), which treats collinear and noncollinear antiferromagnets on the same footing and is expressed in terms of physically measurable parameters instead of molecular-field or exchange coupling constants [1–3]. The influences of magnetic-dipole and single-ion anisotropies and classical anisotropy fields on the magnetic properties of such Heisenberg antiferromagnets were also studied within unified MFT [4–6]. Of particular interest in the context of this MFT are coplanar noncollinear magnetic structures such as those of GdB_4 and triangular antiferromagnets [1,3] and of helical antiferromagnets (see Fig. 1) such as MnO_2 [7] and $MnAu_2$ [8]. More recently the helical antiferromagnets $EuCo_2P_2$ and $EuCo_2As_2$ have been studied for which the MFT provides a good description of the anisotropic magnetic susceptibility below their respective antiferromagnetic (AFM) ordering temperatures T_N [9–12]. Some rare-earth metals also show AFM planar helix or related cone structures [13].

Previously, the magnetic structure and magnetization of a planar helical antiferromagnet in a high applied magnetic fields $\mathbf{H}$ perpendicular to the helix wave vector axis (z axis) at temperature $T = 0$ was calculated where the ordered magnetic moments were restricted to lie in the xy plane [14,15]. This is the plane in which the ordered moments reside in zero field as shown in Fig. 1. This situation corresponds to infinite XY planar anisotropy. Continuous crossover, second-order, and first-order transitions were found between the planar helix and planar fan phases with increasing H [14,15], the nature of which depends on the helix wave vector k. The influence of a high z-axis field on the magnetic moment vectors for the helix phase is shown in Fig. 2. The magnetization versus field for this case was calculated in Ref. [2]. In Ref. [15], the experimental high xy-plane field data at low temperatures T for a single crystal of the helical antiferromagnet $EuCo_2P_2$ [10] containing Eu^{+2} spins $S = 7/2$ were fitted rather well by the theory for $kd = 6\pi/7$, close to the value from neutron-diffraction measurements [9]. However, the presence of a field-induced out-of-plane component of the magnetic moments was not ruled out.

The $T = 0$ calculations were extended to the case of finite XY anisotropy for fields applied perpendicular to the helix axis, where phase transitions between the helix, a three-dimensional spherical ellipse spin-flop (SF), xy fan, and the paramagnetic (PM) phases were found for small turn angles kd [14]. This work was later extended to include study of the magnetic structures at finite temperatures using molecular-field theory [16,17], where the influence of in-plane anisotropy was also studied. Numerical solutions for the in-plane structures at $T = 0$ were also obtained for arbitrary interlayer interactions and arbitrary in-plane anisotropy and applied fields [18]. These treatments are not straightforward to apply to obtain fits of magnetization versus in-plane field data for real materials.

Here we extend the previous $T = 0$ calculations to arbitrary rational kd values for finite classical XY anisotropy

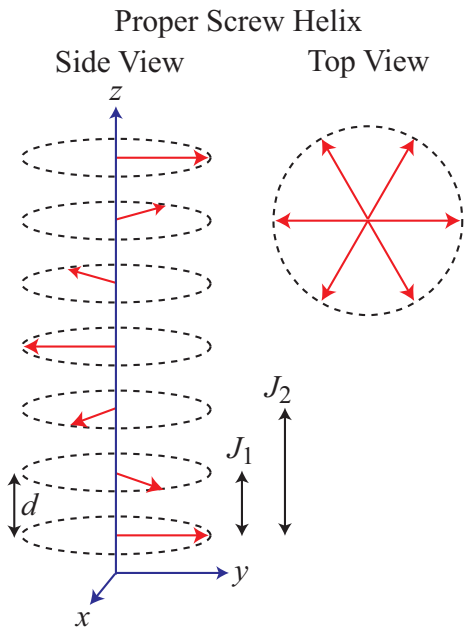

FIG. 1. Generic helical AFM structure [1]. Each arrow represents a layer of moments perpendicular to the z axis that are ferromagnetically aligned within the xy plane and with interlayer separation d. The wave vector $\mathbf{k}$ of the helix is directed along the z axis. The magnetic moment turn angle between adjacent magnetic layers is kd. The nearest-layer and next-nearest-layer exchange interactions J_1 and J_2, respectively, within the J_0-J_1-J_2 Heisenberg MFT model are indicated. The top view is a hodograph of the magnetic moments.

using our formulation of the classical XY anisotropy field $\mathbf{H}_\mathrm{A}$ that was originally developed within unified molecular field theory [6]. We assume that for $\mathbf{H}$ aligned along the x axis, transverse to the helix z axis, the moments can exhibit a transition to one of two types of three-dimensional SF spherical-ellipse phases with increasing H_x with the x axis intersecting the center of each spherical ellipse. One type arises for either ferromagnetic (FM, $J_1 < 0$) or antiferromagnetic (AFM, $J_1 > 0$) nearest-layer interactions J_1 in Fig. 1 and the second type sometimes occurs for AFM J_1 at low H_x and small H_{A1}. All helices have AFM $J_2 > 0$ [2]. The spherical-ellipse nature of the magnetic structures in the SF phase arises from the XY anisotropy and the fixed magnitude of the moments at $T = 0$.

The average energy per spin of a helical spin system with the moments aligned in the xy plane versus H_x in the

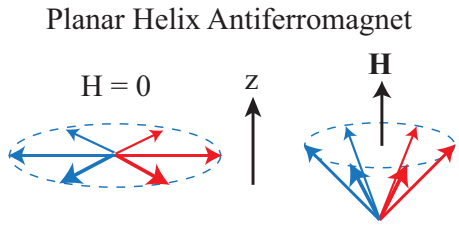

FIG. 2. Hodograph of the magnetic moments in a planar helical structure in the xy plane with applied field (left) $H = 0$, and (right) with a large $\mathbf{H}$ applied along the helix wave-vector z axis [2].

case of infinite XY anisotropy field H_A was calculated for $T = 0$ in Ref. [15]. Here we calculate the average energy per spin at finite H_A, minimized at fixed kd and H_A with respect to the spherical ellipse parameters for the two types of spherical-ellipse SF phases, and compare its energy at each field with that of the planar xy helix/fan phase at the same H_x to determine the stable phase. The PM phase arises naturally from the SF $\rightarrow$ xy fan $\rightarrow$ PM and xy helix $\rightarrow$ xy fan $\rightarrow$ PM phase progression with increasing H_x. This allows the magnetic phase diagram in the H_x–H_A plane at $T = 0$ to be constructed, which we carry out for five values of the turn angle kd. As part of these calculations, we obtain and present the x-axis average magnetic moment per spin $\mu_{x\,\mathrm{ave}}$ versus H_x and H_A for the same five values of kd which also reveal the phase transitions as well as their first- or second-order nature.

The unified MFT used in the present work for both zero and finite temperatures is described in the Appendix, where the general aspects of the theory are reviewed in Sec. A 1 and the application of those to the one-dimensional J_0-J_1-J_2 model (see Fig. 1) is given in Sec. A 2. The model for the SF phase is presented in Sec. II. From minimization of the energy with respect to the SF, xy helix/fan and SF fan phases for five values of kd, the resulting five $T = 0$ phase diagrams in the H_x-H_A plane are presented in Sec. III and Ref. [19], where our previous calculations for the energies of the xy helix/fan phases in Ref. [15] are utilized. The methods needed to interface our theoretical $T = 0$ phase diagrams with experimental low-T magnetization versus field $M(H)$ isotherms and magnetic susceptibility measurements versus T for helical Heisenberg antiferromagnets are presented in detail in Secs. IV A and IV B. A comparison of the phase diagram for $kd = 5\pi/6$ rad with the properties obtained from $M(H)$ isotherm data at $T = 2$ K for $EuCo_2P_2$ with $kd \approx 0.85\pi$ rad [10] is given in Sec. IV C, and reasonable agreement is found. The results of the paper are summarized and discussed in Sec. V.

II. MODEL FOR THE SPIN-FLOP PHASE

The reduced applied magnetic field h_x^{**} and reduced anisotropy field h_{A1}^{**} discussed here are defined in Eqs. (A19). Values of the average energy per spin and the average x-axis magnetic moment per spin versus the reduced field h_x^{**} when the moments in a zero-field helix and high-field fan are confined to the xy plane were calculated for $T = 0$ in Ref. [15]. Here we calculate these $T = 0$ properties for the SF phase where the moments flop out of the xy plane due to a nonzero h_x^{**}. A comparison of the average energy per spin in the helix and SF phases versus h_x^{**} and h_{A1}^{**} will be needed for the construction of the $T = 0$ phase diagrams in the h_x^{**}-h_{A1}^{**} plane.

In the absence of an anisotropy field, in zero applied field a hodograph of the moments in a helix is a circle in the xy plane as shown in Fig. 1. For an infinitesimal h_x^{**}, the moments flop by 90° into the yz plane, thus forming a circular hodograph in the yz plane with an infinitesimal tilt of each spin towards the x axis. However, in the presence of a finite XY anisotropy field h_{A1}^{**}, we assume that the latter circle is flattened into an ellipse in the yz plane where the semimajor axis a of the ellipse is along the y axis and the semiminor axis b is along the z axis,

as found analytically for a special case in Ref. [14]. Due to the fact that we only consider $T = 0$, the moment magnitude μ is fixed at the value given in Eq. (A1c). Hence a hodograph of the moment unit vectors $\hat{\mu}$ in the presence of a nonzero h_x^{**} is a spherical ellipse of radius unity, which is the projection of a two-dimensional ellipse in the yz plane onto a sphere of radius unity. The magnitude μ of the magnetic moments is taken into account in the reduced fields h_x^{**} and $h_{\rm A1}^{**}$.

In the spin-flop phase with finite h_x^{**} and $h_{\rm A1}^{**}$, one expects at least for the case of AFM $J_{12} > 0$ with the applied field in Eq. (A11), that two spherical elliptic paths (hodographs) A and B traversed by the magnetic-moment unit vectors could occur in which the x components have opposite signs in order to decrease the value of exchange interaction energy between spins in adjacent layers. Then the reduced moments with even n in sublattice A are described by

$$\hat{\mu}_{{\rm A}n} = \bar{\mu}_{{\rm A}nx}\,\hat{\mathbf{i}} + \bar{\mu}_{{\rm A}ny}\,\hat{\mathbf{j}} + \bar{\mu}_{{\rm A}nz}\,\hat{\mathbf{k}} \quad (n \text{ even}), \tag{1a}$$

$$\bar{\mu}_{{\rm A}ny} = a_{\rm A}\cos(nkd), \tag{1b}$$

$$\bar{\mu}_{{\rm A}nz} = b_{\rm A}\sin(nkd), \tag{1c}$$

$$\bar{\mu}_{{\rm A}nx} = \sqrt{1 - \left(\bar{\mu}_{{\rm A}ny}^2 + \bar{\mu}_{{\rm A}nz}^2\right)}, \tag{1d}$$

and the moments in sublattice B with odd n are described by

$$\hat{\mu}_{{\rm B}n} = \bar{\mu}_{{\rm B}nx}\,\hat{\mathbf{i}} + \bar{\mu}_{{\rm B}ny}\,\hat{\mathbf{j}} + \bar{\mu}_{{\rm B}nz}\,\hat{\mathbf{k}} \quad (n \text{ odd}), \tag{1e}$$

$$\bar{\mu}_{{\rm B}ny} = a_{\rm B}\cos(nkd), \tag{1f}$$

$$\bar{\mu}_{{\rm B}nz} = b_{\rm B}\sin(nkd), \tag{1g}$$

$$\bar{\mu}_{{\rm B}nx} = c\sqrt{1 - \left(\bar{\mu}_{{\rm B}ny}^2 + \bar{\mu}_{{\rm B}nz}^2\right)}, \tag{1h}$$

where $c = \pm 1$, $n = 1,\ 2,\ \ldots, n_\lambda$, and for each n within each sublattice Eq. (A1f) is satisfied. The moments are distributed in equal numbers between sublattices A and B, labeled by consecutive odd and even integers n, respectively, so the total number of moments n_λ per wavelength $\lambda = n_\lambda d$ along the z axis is even. An illustration of the spherical ellipse paths of the moments on sublattices A and B described by Eqs. (1) is shown in Fig. 3 for $c = -1$, $a_{\rm A} = a_{\rm B} = 0.8$ and $b_{\rm A} = b_{\rm B} = 0.2$. The value $c = -1$ corresponds to two spherical-elliptic paths on opposite sides of $\bar{\mu}_x = 0$ for sublattices A and B as shown in the figure. This may be expected at small h_x^{**} for AFM $J_1 > 0$, whereas when $c = 1$, the paths are on the same side of the positive $\bar{\mu}_x$ axis towards which the applied magnetic field **H** points, as expected for all moments for large h_x^{**} with either AFM or FM J_1.

The spherical-ellipse parameters c, $a_{\rm A}$, $b_{\rm A}$, $a_{\rm B}$, $b_{\rm B}$ are all determined at the same time by minimizing the normalized average energy per spin $E_{\rm ave}/(S^2J_2)$ in Eq. (A20b) with respect to these parameters in Eqs. (1) when inserted into Eq. (A20a) for fixed values of $h_{\rm A1}^{**}$ and h_x^{**}. If the obtained values satisfy $c = -1$ or $c = 1$ with $a_{\rm A} \neq a_{\rm B}$, $b_{\rm A} \neq b_{\rm B}$, then there are two spherical ellipses, one on each side of $\bar{\mu}_x = 0$ if $c = -1$ and both on the $\bar{\mu}_x > 0$ side if $c = 1$. On the other hand, if $b_{\rm A}$ and $b_{\rm B}$ satisfy $b_{\rm A} = b_{\rm B} = 0$ (no z-axis component to the moments), either one ($a_{\rm A} = a_{\rm B}$) or two ($a_{\rm A} \neq a_{\rm B}$) xy fan phases are found. Finally, if $a_{\rm A} = a_{\rm B} = b_{\rm A} = b_{\rm B} = 0$, the moments all point in the direction of the applied field in the $+x$ direction and the system is in the PM state.

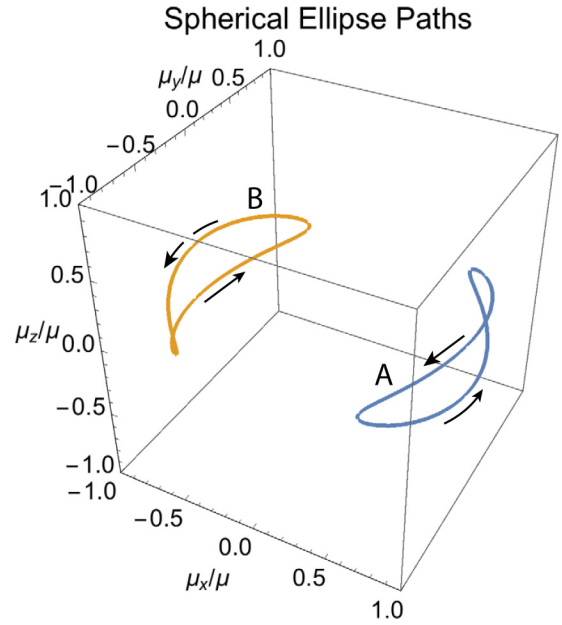

FIG. 3. Spherical-ellipse paths (hodographs) of the magnetic moment unit vectors $\vec{\mu}/\mu$ in sublattices A and B in the spin-flop (SF) phase according to Eqs. (1) with the parameter $c = -1$. These paths are elliptical in the yz plane with a constant radius of unity from the origin of the Cartesian coordinate system. In this illustration, the semimajor and semiminor axes of the elliptic paths in the yz plane are set to $a_{\rm A} = a_{\rm B} = 0.8$, $b_{\rm A} = b_{\rm B} = 0.2$, but the equalities $a_{\rm A} = a_{\rm B}$ and $b_{\rm A} = b_{\rm B}$ are generally not obtained for the SF phase from energy minimization even when $c = 1$ and the spherical ellipses are both on the positive side of $x = 0$ towards which the applied magnetic field **H** points.

Once the spherical-ellipse parameters are determined, the average value of x component of the magnetic moment unit vector in the direction of the applied field for the given values of h_x^{**} and $h_{\rm A1}^{**}$ is obtained from

$$\bar{\mu}_{x\rm ave} \equiv \frac{\mu_{x\rm ave}}{\mu} = \frac{1}{n_\lambda}\sum_{n=1}^{n_\lambda}\bar{\mu}_{nx} \tag{2}$$

using Eqs. (1d) and (1h).

The fitted values of $E_{\rm ave}/(S^2J_2)$, $\bar{\mu}_{x\rm ave}$, and of c, $a_{\rm A}$, $b_{\rm A}$ $a_{\rm B}$, $b_{\rm B}$ are shown for representative values $kd = \pi/6$ and $\pi/4$; $\pi/3$ and $3\pi/7$; $13\pi/25$ and $5\pi/9$; and $9\pi/11$ and $5\pi/6$; in Ref. [19]. One sees a variety of possible SF phases for different values of $h_{\rm A1}^{**}$ and of h_x^{**}, including a single spherical ellipse, a single xy fan, two spherical ellipses, two xy fans, and at high fields, the PM phase in which all moments are FM-aligned in the direction $\hat{\mathbf{i}}$ of the applied field. There is no clear monotonic dependence versus kd in the order in which the first four phases occur. A nonmonotonic behavior versus kd was previously found in the range $4\pi/9 \leqslant kd < \pi$ for the phases occurring at $T = 0$ versus applied x-axis field for the xy helix and xy fan phases when the moments are confined to the xy plane [15]. The stable phases for $0 < kd < \pi/2$ with FM (negative) J_{12} all have $c = 1$ for all h_x^{**} as anticipated, whereas two of the stable phases for $\pi/2 < kd < \pi$ with AFM (positive) J_{12}

have $c = -1$ at low fields, as also anticipated, and $c = 1$ at high fields.

First-order transitions versus h_x^{**} occur when c discontinuously changes with increasing h_x^{**} from -1 to 1 in Ref. [19] for $kd = 9\pi/11$ and $kd = 5\pi/6$. The first-order nature of the transitions is also revealed in the h_x^{**} dependencies of $E_{\rm ave}$, $\bar{\mu}_{x\,\rm ave}$ and the other four spherical ellipse parameters. The transitions versus h_x^{**} for the other six kd values in Ref. [19] are seen to be second order. When kd increases from $9\pi/11$ to $5\pi/6$, both with $h_{\rm A1}^{**} = 1$ in Ref. [19], a new second-order transition at $h_1^{**} = 1.0$ occurs for $kd = 5\pi/6$, whereas for $kd = 9\pi/11$ the transition is instead a smooth crossover.

The reduced critical field $h_{\rm c}^{**}$ versus kd is the value at which the system becomes PM with increasing h_x^{**}. These second-order transition fields are listed for each of the eight kd values and the specified values of $h_{\rm A1}^{**}$ in Ref. [19]. We find that $h_{\rm c}^{**}$ depends only on kd (not on $h_{\rm A1}^{**}$), when n_λ is even as assumed in this paper. For $h_x^{**} \to h_{\rm c}^{**-}$, the stable phase for all values of kd is a single fan in the xy plane, which was studied in detail in Ref. [15]. The approximate values of $h_{\rm c}^{**}$ versus kd listed in the figures in Ref. [19] are in agreement with the respective exact values given for the xy fan by [15]

$$h_{\rm c}^{**} = 16\sin^4\left(\frac{kd}{2}\right). \tag{3}$$

III. PHASE DIAGRAMS IN THE h_x^{**}-$h_{\rm A1}^{**}$ PLANE FOR REPRESENTATIVE kd VALUES

As discussed above, the phases that can occur within MFT are the xy helix phase with moments aligned in the xy plane (xy helix/fan), the spin-flop (SF) phase with moments that have three-dimensional components (xyz spin flop), the xy fan phase with moments oriented within the xy plane (SF xy fan) and the paramagnetic (PM) phase where the moments are ferromagnetically aligned in the direction of the x-axis reduced field h_x^{**}.

The phase boundary between the xy helix phase and the xy fan phase of the helix when it occurs was determined previously in Ref. [15], where the energies of the xy helix and higher-field xy fan phases were determined versus h_x^{**}. However, here one needs to determine the influence of $h_{\rm A1}^{**}$ on those energies. Since these moments are confined to the xy plane, the reduced energy of moment layer n for the xy helix and associated high-field xy fan phases is given by Eq. (A20a) as

$$\frac{E_n^{\rm helix/fan}}{S^2J_2} = \frac{1}{2}[J_{12}(\hat{\mu}_n\cdot\hat{\mu}_{n+1} + \hat{\mu}_n\cdot\hat{\mu}_{n-1}) + (\hat{\mu}_n\cdot\hat{\mu}_{n+2} + \hat{\mu}_n\cdot\hat{\mu}_{n-2})] - (h_{\rm A1}^{**} + \bar{\mu}_{nx}h_x^{**}) \tag{4a}$$

$$= \frac{E_n^{\rm helix/fan}}{S^2J_2}(h_x^{**}, h_{\rm A1}^{**} = 0) - h_{\rm A1}^{**}, \tag{4b}$$

where the first term on the right-hand side of the bottom equality was calculated for a variety of turn angles kd in Ref. [15].

One anticipates that when $h_{\rm A1}^{**} = 0$, in order for the system to minimize its energy an infinitesimal h_x^{**} causes the xy helix to immediately spin-flop to a perpendicular orientation in the yz plane. With further increases in h_x^{**}, the moments all tilt by the same angle towards the x axis as shown in Fig. 2 where the z axis in that figure is replaced by the x axis here. When $h_{\rm A1}^{**}$ increases to a finite value, one expects a finite field to be required to cause the moments to flop out of the xy plane to enter the SF phase. However, if $h_{\rm A1}^{**}$ is sufficiently large, this xy helix to xyz spin-flop transition is expected to be replaced by the previously studied xy helix to xy fan phase transition. These expectations are borne out by the phase diagrams shown in Ref. [19] and Fig. 4(c) below.

The reduced phase transition field h_x^{**} between the xy helix phase and the xyz spin-flop phase for a given value of reduced XY anisotropy field $h_{\rm A1}^{**}$ was determined by the crossover in average energy between these two phases, where at low fields the xy helix phase has the lower energy and at higher fields the xyz spin-flop phase energy is lower. This is a first-order transition. The transition between the xy helix phase and the high-field xy helix fan phase can be first-order, second-order, or a smooth crossover [15]. The phase transition field between the xyz SF and the PM phases or between the xy SF fan phase and the PM phase are determined by the criterion that the x component of the calculated average moment unit vector per spin $\bar{\mu}_{x\,\rm ave} \equiv \mu_{x\,\rm ave}/\mu$ becomes equal to unity with increasing h_x^{**}. This is a continuous (second-order) transition.

The phase diagrams in the $h_x^{**} - h_{\rm A1}^{**}$ plane at $T = 0$ calculated for the four turn angles $kd = \pi/6,\ \pi/4,\ \pi/3$, and $3\pi/4$ rad are shown in Ref. [19]. The first three turn angles correspond to FM nearest-layer couplings $J_1 < 0$ whereas the fourth one is for an AFM $J_1 > 0$. One sees that the phase diagrams follow the above expectations. The first three phase diagrams with FM $kd < \pi/2$ have common forms, where approximately the same phase diagram is obtained but with a rescaling of the h_x^{**} and $h_{\rm A1}^{**}$ axes. In all three phase diagrams the phase transition line between the xyz spin flop and the xy fan phases is linear or nearly so. Another interesting feature is that all three phase diagrams show a horizontal first-order xy helix to xy fan phase boundary at large $h_{\rm A1}^{**}$ values. This occurs at the respective first-order transition fields $h_{\rm t}^{**}$ between these two xy phases reported previously in Ref. [15]. These three phase diagrams are similar in form to the $T = 0$ phase diagram in Fig. 4 of Ref. [14] for small values of kd. The phase diagram for $kd = 3\pi/4$ in Ref. [19] for $kd > \pi/2$ corresponding to AFM $J_1 > 0$ is different from the other figures where the nearest-layer coupling is FM. In Fig. 4, the phase diagram and other data for $kd = 5\pi/6$ are shown which will be compared with experimental data for $EuCo_2P_2$ in the following section.

We emphasize that the transitions versus h_x^{**} at fixed $h_{\rm A1}^{**}$ for the SF phase shown in Ref. [19] and Fig. 4(c) for particular values of kd are only observed in a real helical Heisenberg AFM compound if the SF phase has a lower energy than each of the xy helix and xy helix fan phases for the particular values of kd, $h_{\rm A1}^{**}$ and range of h_x^{**} that are associated with the compound. Indeed, we show that for the model helical Heisenberg antiferromagnet $EuCo_2P_2$ discussed in Sec. IV C below, the values of kd and $h_{\rm A1}^{**}$ do not allow the SF phase to have a lower energy than the xy helix or xy helix fan phases for any value of h_x^{**}. Hence only the xy helix, xy helix fan, and PM phases occur with increasing h_x^{**}.

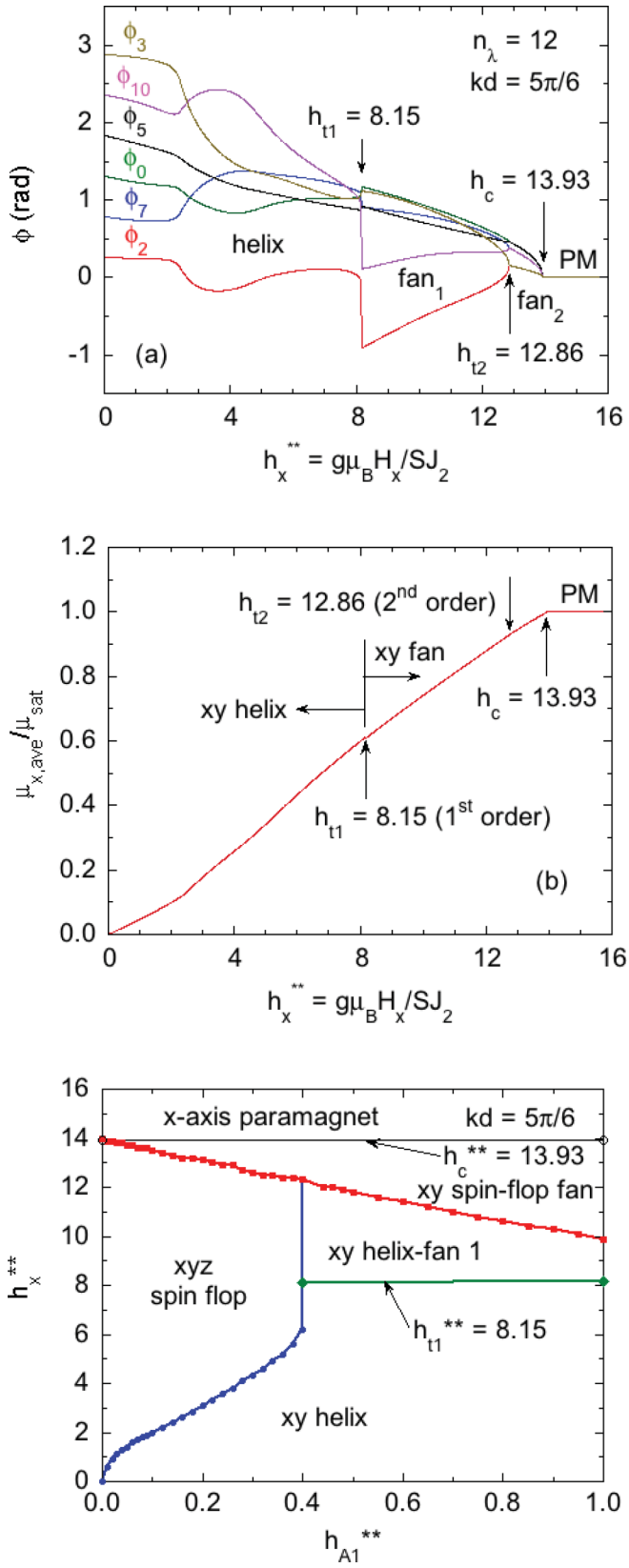

FIG. 4. (a) Phase angles ϕ_n ($n = 2, 7, 0, 5, 10, 3$) with respect to the positive x axis of the six inequivalent moments in a helix with $kd = 5\pi/6$ confined to the xy plane at $T = 0$ in the notation of Ref. [15]. (b) Average x-axis moment vs h_x^{**} calculated from the data in (a). The data in (a) and (b) were not presented in Ref. [15]. (c) Phase diagram in the h_x^{**}-h_{A1}^{**} plane at $T = 0$.

IV. COMPARISON OF THE THEORY WITH EXPERIMENT

A. Expressing h_{A1}^{**} and h_x^{**} in terms of experimental values of h_{A1} and h_x

In order to compare experimental magnetic data for helical Heisenberg antiferromagnets with the above theory, one needs to determine which region of the phase diagram (xy helix phase, xy helix fan phase, xyz SF phase, xy SF fan phase, or PM phase) a material lies for the material's values of h_x^{**} and h_{A1}^{**}. Then one can compare the experimental $M(H)$ data for the compound at low T with the theoretical phase diagrams to determine what phase transitions are predicted versus x-axis field for comparison with the experimental $M(H)$ data.

To accomplish this comparison, one must first determine how the value of the reduced applied field h_x^{**} and anisotropy field h_{A1}^{**} in this paper are expressed in terms of the reduced applied field h_x and reduced anisotropy field h_{A1} defined in Ref. [6] that can be obtained from experimental magnetic susceptibility data (see following section). From Ref. [6], one has

$$h_{A1} \equiv \frac{g\mu_B H_{A1}}{k_B T_{NJ}}, \tag{5a}$$

where k_B is Boltzmann's constant and T_{NJ} is the Néel temperature that would be obtained from Heisenberg exchange interactions alone with no anisotropy contributions. A comparison of this definition with that for h_{A1}^{**} in Eq. (A19b) gives the conversion

$$h_{A1}^{**} = \left[\frac{3}{2S(S+1)}\right]\left(\frac{k_B T_{NJ}}{J_2}\right)h_{A1}. \tag{5b}$$

Similarly, a comparison of the definition [6]

$$h_x \equiv \frac{g\mu_B H_x}{k_B T_{NJ}} \tag{5c}$$

with that for h_x^{**} in Eq. (A19a) yields

$$h_x^{**} = \frac{1}{S}\left(\frac{k_B T_{NJ}}{J_2}\right)h_x. \tag{5d}$$

These conversions require the spin S to be known and also the material-specific ratio $k_B T_{NJ}/J_2$ within the J_0-J_1-J_2 MFT model to be computed from magnetic susceptibility data for single crystals of the material. The latter calculation also yields J_0 and J_1 as discussed in the following section.

B. Extracting values of h_{A1}, T_{NJ}, J_0, J_1, ad J_2 from experimental magnetic susceptibility data within unified molecular-field theory

The value of the experimental XY anisotropy parameter h_{A1} is estimated from the anisotropy in the experimental Weiss temperatures $\theta_{p\alpha}$ in the Curie-Weiss law fitted to magnetic susceptibility data in the PM state of uniaxial single crystals according to [6]

$$\theta_{p\,ab} - \theta_{p\,c} = T_N\left(\frac{h_{A1}}{1 + h_{A1}}\right), \tag{6}$$

where the ab crystal plane corresponds to the xy plane in the theory and the c axis to the z axis, and T_N is the measured Néel temperature including both exchange and anisotropy

contributions. Then the Néel temperature T_{NJ} due to exchange interactions alone is found from

$$T_{NJ} = \frac{T_N}{1 + h_{A1}}. \tag{7}$$

The Weiss temperature θ_{pJ} in the Curie-Weiss law due to exchange interactions alone is the spherical average

$$\theta_{pJ} = \frac{2\theta_{p\,ab} + \theta_{p\,c}}{3} \tag{8}$$

of the measured values $\theta_{p\,ab}$ and $\theta_{p\,c}$.

Once T_{NJ} and θ_{pJ} are determined for a particular compound, one can determine the parameters J_0, J_1, and J_2 within the J_0-J_1-J_2 MFT model by solving for them from the three simultaneous equations [2]

$$\begin{aligned} \cos(kd) &= -\frac{J_1}{4J_2}, \\ \theta_{pJ} &= -\frac{S(S+1)}{3}(J_0 + 2J_1 + 2J_2), \\ T_{NJ} &= -\frac{S(S+1)}{3}[J_0 + 2J_1\cos(kd) + 2J_2\cos(2kd)], \end{aligned} \tag{9}$$

where $J_2 > 0$, the J_i are expressed here in temperature units, and the turn angle kd is assumed to be known from neutron diffraction measurements and/or from fitting the xy-plane magnetic susceptibility below T_N by MFT [1–3]. The solutions for J_0, J_1, and J_2 obtained from Eqs. (9) are

$$\begin{aligned} J_0 = &-\frac{3\csc^4(kd/2)}{8S(S+1)}\{T_{NJ}[1 - 4\cos(kd)] \\ &+ \theta_{pJ}[2 + \cos(2kd)]\}, \end{aligned} \tag{10a}$$

$$J_1 = -\frac{3\csc^4(kd/2)}{4S(S+1)}(T_{NJ} - \theta_{pJ})\cos(kd), \tag{10b}$$

$$J_2 = \frac{3\csc^4(kd/2)}{16S(S+1)}(T_{NJ} - \theta_{pJ}). \tag{10c}$$

C. Application to the model molecular-field helical Heisenberg antiferromagnet $EuCo_2P_2$

$EuCo_2P_2$ is a model MFT helical Heisenberg antiferromagnet with the Eu^{+2} spins situated on a body-centered-tetragonal sublattice with properties given by [10]

$$S = 7/2, \tag{11a}$$

$$T_N = 66.6\ \text{K}, \tag{11b}$$

$$kd = 0.852\pi\ \text{rad}, \tag{11c}$$

$$\theta_{p\,ab} = 23.0\ \text{K}, \tag{11d}$$

$$\theta_{p\,c} = 18.2\ \text{K} \tag{11e}$$

where the value of kd was obtained by neutron diffraction measurements at $T = 15\ \text{K} \ll T_N$ [9] and is close to the value $kd = 5\pi/6 = 0.833\pi$ in Fig. 4. Using $g = 2$ and Eqs. (5c) and (7) to (10), one obtains

$$h_{A1} = 0.078, \tag{12a}$$

$$T_{NJ} = 61.8\ \text{K}, \tag{12b}$$

$$J_0/k_B = -9.0\ \text{K}, \tag{12c}$$

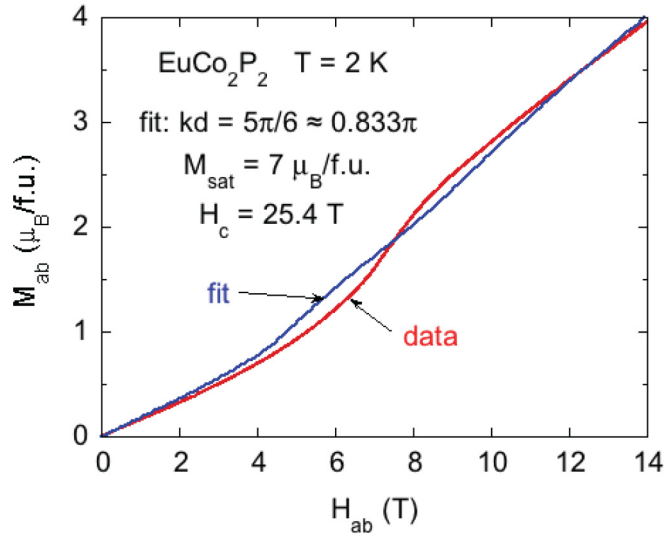

FIG. 5. High-field magnetization M_{ab} vs magnetic field H applied in the crystallographic ab plane (the xy plane in the theory here) perpendicular to the helix c (z) axis [10]. The saturation moment is $M_{sat} = gS\mu_B$, where the spectroscopic splitting factor is taken to be $g = 2$, the Eu^{+2} spin to be $S = 7/2$, and μ_B is the Bohr magneton.

$$J_1/k_B = 1.92\ \text{K}, \tag{12d}$$

$$J_2/k_B = 0.54\ \text{K}, \tag{12e}$$

$$h_{A1}^{**} = 11.0h_{A1} = 0.85, \tag{12f}$$

$$h_x^{**} = 32.9h_x = 0.72H_x[\text{T}], \tag{12g}$$

$$\begin{aligned} h_c^{**} &= 32.9h_c \\ &= 0.72H_c[\text{T}], \end{aligned} \tag{12h}$$

where 1 T $= 10^4$ Oe. The negative value of J_0 is consistent with the FM alignment of the moments in each helix layer, and the positive values of J_1 and J_2 indicate AFM interlayer couplings with $J_2 < J_1$ as would be expected. A positive AFM value of J_2 is required to form a helix structure. Using Eqs. (3) and (12h) and the value of kd in Eq. (11c), one obtains predictions for the reduced and actual critical fields as

$$h_c^{**} = 15.6, \tag{13a}$$

$$H_c = 21.7\ \text{T} \tag{13b}$$

The value for H_c is close to the fitted value of 25.4 T obtained in the following.

The value $h_{A1}^{**} = 0.85$ in Eq. (12f) places $EuCo_2P_2$ near the right edge of the phase diagram in Fig. 4(c) where a weakly first-order transition from the xy helix phase to the xy fan phase occurs at a field of 58.5% of the critical field. We first fit the experimental $M_{ab}(H)$ data for a single crystal with the applied field in the ab (i.e., xy) plane shown in Fig. 5 to obtain an estimate of the critical field H_c. Using the prediction of $M(H)$ for $kd = 5\pi/6 = 0.833\pi$ in Fig. 4(b), the fit shown in Fig. 5 is obtained with the fitted value

$$H_c = 25.4\ \text{T}. \tag{14}$$

The fit semiquantitatively reproduces the overall upward curvature of the data, although the S-shape centered in the data at ≈7 T occurs at a somewhat higher field than the value

of ≈5 T in the fit. Not surprisingly, a similar-quality fit was previously obtained assuming $kd = 6\pi/7 \approx 0.857\pi$ for the helix/fan phase confined to the xy plane [15].

V. SUMMARY AND DISCUSSION

The present work is a continuation of the development and use of the unified molecular field theory for systems containing identical crystallographically-equivalent Heisenberg spins [1–3]. This MFT has significant advantages over the previous Weiss MFT because it treats collinear and noncollinear AFM structures on the same footing and the variables in the theory are expressed in terms of directly measurable experimental quantities instead of ill-defined molecular-field coupling constants or Heisenberg exchange interactions.

As part of this development, the influences of several types of anisotropies on the magnetic properties of Heisenberg antiferromagnets were calculated [4–6], including a classical anisotropy field [6] that was used to good advantage in the present work. This allowed the transverse-field dependence of the spin-flop phases of helical antiferromagnets to be easily calculated in the presence of finite XY anistropy. The present work allowed the possibility of either one or two coexisting spherical elliptical hodographs of the moments in the spin-flop phase that enhanced the flexibility for the system to attain a minimum energy versus applied and anisotropy fields.

Together with the previous work on the xy helix and xy fan phases that occur under x-axis fields and their corresponding energies at $T = 0$ [15], the present results on the spin-flop and associated fan energies were utilized to construct x-axis field H_x versus anisotropy field H_{A1} phase diagrams that can be compared directly with low-T experimental magnetization versus transverse field data for helical antiferromagnets. Care was taken to explain how to do this. Then a comparison of the theory with the magnetic behavior of the model MFT helical Heisenberg antiferromagnet $EuCo_2P_2$ was carried out. Semiquantitative agreement was found and the value of the extrapolated critical field H_c was determined.

A previous theoretical study was reported of the helix-to-fan transition at $T = 0$ that occurs with increasing x-axis magnetic field transverse to the helix z axis when the local moments are confined to the xy plane [14]. These authors also calculated the transverse field versus XY anisotropy phase diagram as in our Fig. 4(c) and Ref. [19] but for small values of the helix turn angle kd where the moments spin-flop out of the xy plane into a single spherical ellipse phase with the axis of the spherical ellipse parallel to the applied transverse field [14]. In the present work the range of kd was extended and the SF phase contained either one or two spherical ellipses instead of one. For $0 < kd < \pi/2$ rad, the topology of our phase boundaries and the phases themselves are similar to theirs. However, we found significant differences between the phase diagrams for $kd = 3\pi/4$ and $5\pi/6$ and the phase diagrams for $kd < \pi/2$ rad.

Since the theoretical predictions were obtained using MFT, quantum fluctuations are not taken into account and hence the predictions are expected to be most accurate for helical Heisenberg antiferromagnets containing large spins such as Mn^{+2} ions with spin $S = 5/2$ and Gd^{+3} and Eu^{+2} ions with $S = 7/2$. Although the calculated phase diagrams are for $T = 0$, in practice this means that experimental data with which the theoretical phase diagrams are compared should include data at temperatures much lower than the AFM ordering (Néel) temperature, a restriction that is often easy to accommodate as in the presently-examined case of $EuCo_2P_2$. Future work could profitably include classical ground-state Monte Carlo simulations to test our model for the spin-flop phase and associated field-dependent magnetization.

ACKNOWLEDGMENTS

The author is grateful to N. S. Sangeetha for discussions and collaboration on the model MFT helical Heisenberg antiferromagnet $EuCo_2P_2$ that motivated this work. This research was supported by the U.S. Department of Energy, Office of Basic Energy Sciences, Division of Materials Sciences and Engineering. Ames Laboratory is operated for the U.S. Department of Energy by Iowa State University under Contract No. DE-AC02-07CH11358.

APPENDIX: THEORY

1. General theory

All spins are assumed to be identical and crystallographically equivalent which means that they each have the same magnetic environment. The magnetic moment $\vec{\mu}_n$ of spin n is

$$\vec{\mu}_n = -g\mu_B \mathbf{S}_n \tag{A1a}$$

where the negative sign arises from the negative charge on an electron, g is the spectroscopic splitting factor of each moment, μ_B is the Bohr magneton, and $\mathbf{S}_n$ is the spin angular momentum of $\vec{\mu}_n$ in units of $\hbar$ which is Planck's constant h divided by 2π. One can also write

$$\vec{\mu}_n = \mu\,\hat{\mu}_n, \tag{A1b}$$

where $\mu = |\vec{\mu}|$. At $T = 0$ as considered in this paper, μ is the saturation moment given from Eq. (A1a) as

$$\mu = g\mu_B S. \tag{A1c}$$

In Cartesian coordinates, the unit vector $\hat{\mu}_n$ in the direction of $\vec{\mu}_n$ is written as

$$\hat{\mu}_n = \bar{\mu}_{nx}\,\hat{\mathbf{i}} + \bar{\mu}_{ny}\,\hat{\mathbf{j}} + \bar{\mu}_{nz}\,\hat{\mathbf{k}}, \tag{A1d}$$

where the Cartesian unit vectors pointing towards the positive x, y, and z directions are $\hat{\mathbf{i}}$, $\hat{\mathbf{j}}$, and $\hat{\mathbf{k}}$, respectively, and

$$\bar{\mu}_{nx,ny,nz} \equiv \frac{\mu_{nx,ny,nz}}{\mu}. \tag{A1e}$$

Therefore

$$\hat{\mu}_n \cdot \hat{\mu}_n = 1 = \bar{\mu}_{nx}^2 + \bar{\mu}_{ny}^2 + \bar{\mu}_{nz}^2. \tag{A1f}$$

The energy per spin E_n of a representative spin $\mathbf{S}_n$ interacting with its neighbors $\mathbf{S}_{n'}$ and with the classical anisotropy field $\mathbf{H}_{An}$ and applied magnetic field $\mathbf{H}$ is

$$E_n = E_{exchn} + E_{An} + E_{Hn}. \tag{A2}$$

The Heisenberg exchange energy per spin E_{exchn} is [2]

$$E_{exchn} = \frac{1}{2}\mathbf{S}_n \cdot \sum_{n'} J_{nn'}\mathbf{S}_{n'}, \tag{A3}$$

where the prefactor of 1/2 is due to the fact that the exchange energy from interaction between a pair of spins is equally shared between the members of the pair, and $J_{nn'}$ is the Heisenberg exchange interaction between spins $\mathbf{S}_n$ and $\mathbf{S}_{n'}$. Writing the classical expression

$$\mathbf{S}_n \cdot \mathbf{S}_{n'} = S^2 \cos\alpha_{nn'}, \tag{A4}$$

where $\alpha_{nn'}$ is the angle between $\vec{\mu}_n$ and $\vec{\mu}_{n'}$, Eq. (A3) becomes

$$E_{\mathrm{exch}n} = \frac{S^2}{2}\sum_{n'} J_{nn'}\cos\alpha_{nn'}. \tag{A5}$$

In terms of the magnetic moments, this can be written

$$E_{\mathrm{exch}n} = \frac{S^2}{2}\sum_{n'} J_{nn'}\hat{\mu}_n \cdot \hat{\mu}_{n'}. \tag{A6}$$

The anisotropy energy $E_{\mathrm{A}n}$ is assumed to arise from a classical anisotropy field $\mathbf{H}_{\mathrm{A}n}$ originating fundamentally from two-spin interactions (i.e., not from single-ion anisotropy) that is given by [6]

$$E_{\mathrm{A}n} = -\frac{1}{2}\vec{\mu}_n \cdot \mathbf{H}_{\mathrm{A}n} = -\frac{\mu}{2}\hat{\mu}_n \cdot \mathbf{H}_{\mathrm{A}n}, \tag{A7}$$

where the prefactor of 1/2 arises for the same reason as in Eq. (A3). The $\mathbf{H}_{\mathrm{A}n}$ seen by $\vec{\mu}_n$ is proportional to the projection of $\hat{\mu}_n$ onto the xy plane according to [6]

$$\mathbf{H}_{\mathrm{A}n} = \frac{3H_{\mathrm{A1}}}{S+1}(\bar{\mu}_{nx}\hat{\mathbf{i}} + \bar{\mu}_{ny}\hat{\mathbf{j}}), \tag{A8}$$

where H_{A1} is the so-called fundamental anisotropy field. Inserting Eqs. (A1d) and (A8) into (A7) and using Eq. (A1c) gives

$$\begin{aligned} E_{\mathrm{A}n} &= -\frac{3S}{2(S+1)}g\mu_{\mathrm{B}}H_{\mathrm{A1}}\left(\bar{\mu}_{nx}^2 + \bar{\mu}_{ny}^2\right) \\ &= -\frac{3S}{2(S+1)}g\mu_{\mathrm{B}}H_{\mathrm{A1}}\left(1 - \bar{\mu}_{nz}^2\right), \end{aligned} \tag{A9}$$

where the second equality was obtained using Eq. (A1f).

The Zeeman energy E_{Hn} of $\vec{\mu}_n$ in the applied magnetic field $\mathbf{H}$ is

$$E_{Hn} = -\vec{\mu}_n \cdot \mathbf{H} = -\mu\bar{\mu}_{nx}H_x = -g\mu_{\mathrm{B}}S\bar{\mu}_{nx}H_x, \tag{A10}$$

where Eqs. (A1c) and (A1d) were used and $\mathbf{H}$ is assumed to be applied in the $\hat{\mathbf{i}}$ direction, transverse to the helix z axis, i.e.,

$$\mathbf{H} = H_x\hat{\mathbf{i}}. \tag{A11}$$

Inserting Eqs. (A6), (A9), and (A10) into (A2) gives the energy per spin as

$$\begin{aligned} E_n = \frac{S^2}{2}\sum_{n'} J_{nn'}\hat{\mu}_n \cdot \hat{\mu}_{n'} - \frac{3S}{2(S+1)}g\mu_{\mathrm{B}}H_{\mathrm{A1}}\left(1 - \bar{\mu}_{nz}^2\right) \\ - \bar{\mu}_{nx}Sg\mu_{\mathrm{B}}H_x. \end{aligned} \tag{A12}$$

2. J_0-J_1-J_2 one-dimensional MFT model for the exchange energy of helical antiferromagnets

The J_0-J_1-J_2 unified MFT model for the Heisenberg exchange interactions [1,2] is utilized to treat helical structures such as illustrated in Fig. 1, where J_0 is the sum of all Heisenberg exchange interactions between a representative spin $\mathbf{S}_n$ in a FM-aligned layer with all other spins in the same layer, J_1 is the sum of the interactions of that spin with all spins in a nearest-neighbor layer, and J_2 is the sum of the interactions of that spin with all spins in a next-nearest-neighbor layer, as shown in Fig. 1. Within this MFT model, the exchange energy of a representative spin $\mathbf{S}_n$ with magnitude S interacting with its neighbors is given by Eq. (A5) for $H_x = 0$ and with spins confined to the xy plane as

$$E_{\mathrm{exch}n} = \frac{S^2}{2}[J_0 + 2J_1\cos(kd) + 2J_2\cos(2kd)], \tag{A13}$$

where $J_{nn'}$ and α_{ji} in Eq. (A5) are defined as J_1 and kd for a nearest-neighbor layer and by J_2 and $2kd$ for a next-nearest-neighbor layer, respectively, k is the magnitude of the helix wave vector along the z axis and d is the distance between layers as shown in Fig. 1. The prefactors of two in the last two terms occur because each layer has two nearest-layer neighbors and two next-nearest-layer neighbors. The turn angle kd between adjacent FM-aligned layers in the helix in zero applied field is given in terms of J_1 and J_2 by [2]

$$\cos(kd) = -\frac{J_1}{4J_2}, \tag{A14}$$

which we utilize in subsequent calculations in this paper.

This paper is particularly concerned with spin-flop phases that can arise from an external field H_x that is perpendicular to the helix z axis for which the moments are not confined to the xy plane but also have z components. In that case, we still assume that all moments in a layer perpendicular to the helix z axis are FM aligned, but that the z component can vary from layer to layer. Therefore, for the spin-flop phase, the exchange energy per spin in Eq. (A13) is generalized to read

$$\begin{aligned} E_{\mathrm{exch}n} = \frac{S^2}{2}[J_0 + J_1\hat{\mu}_n \cdot (\hat{\mu}_{n+1} + \hat{\mu}_{n-1}) \\ + J_2\hat{\mu}_n \cdot (\hat{\mu}_{n+2} + \hat{\mu}_{n-2})]. \end{aligned} \tag{A15}$$

This equation reduces to Eq. (A13) if the z components of the $\hat{\mu}_i$ are zero and the turn angle between the moments in adjacent layers is kd as in the helix in Fig. 1 when the external applied field is $H_x = 0$.

It is convenient to normalize all exchange constants by J_2 because $J_2 > 0$ for a helix [2]. Defining the dimensionless ratios

$$J_{02} \equiv \frac{J_0}{J_2}, \quad J_{12} \equiv \frac{J_1}{J_2}, \quad J_{22} \equiv \frac{J_2}{J_2} \equiv 1, \tag{A16}$$

Eq. (A15) becomes

$$\begin{aligned} E_{\mathrm{exch}n} = \frac{S^2J_2}{2}[J_{02} + J_{12}\hat{\mu}_n \cdot (\hat{\mu}_{n+1} + \hat{\mu}_{n-1}) \\ + \hat{\mu}_n \cdot (\hat{\mu}_{n+2} + \hat{\mu}_{n-2})]. \end{aligned} \tag{A17}$$

Then normalizing all energies by S^2J_2 [15], Eq. (A12) for the energy per spin now reads

$$\frac{E_n}{S^2J_2} = \frac{1}{2}[J_{02} + J_{12}\hat{\mu}_n \cdot (\hat{\mu}_{n+1} + \hat{\mu}_{n-1}) + \hat{\mu}_n \cdot (\hat{\mu}_{n+2} + \hat{\mu}_{n-2})] - \frac{3S}{2(S+1)}\frac{g\mu_B H_{A1}}{S^2J_2}\left(1 - \bar{\mu}_{nz}^2\right) - \bar{\mu}_{nx}S\frac{g\mu_B H_x}{S^2J_2}. \quad \text{(A18)}$$

Dimensionless reduced magnetic fields are defined as

$$h_x^{**} = \frac{g\mu_B H_x}{SJ_2}, \quad \text{(A19a)}$$

$$h_{A1}^{**} = \frac{3S}{2(S+1)}h_{A1}^{*}, \quad \text{(A19b)}$$

$$h_c^{**} = \frac{g\mu_B H_c}{SJ_2} \quad \text{(A19c)}$$

where the last expression is the reduced critical field discussed in Sec. II. Using Eqs. (A19), the normalized energy in Eq. (A18) becomes

$$\frac{E_n}{S^2J_2} = \frac{1}{2}[J_{02} + J_{12}\hat{\mu}_n \cdot (\hat{\mu}_{n+1} + \hat{\mu}_{n-1}) + \hat{\mu}_n \cdot (\hat{\mu}_{n+2} + \hat{\mu}_{n-2})] - \left[h_{A1}^{**}\left(1 - \bar{\mu}_{nz}^2\right) + \bar{\mu}_{nx}h_x^{**}\right]. \quad \text{(A20a)}$$

Thus a nonzero out-of-plane component $\bar{\mu}_{nz}$ of a moment unit vector $\hat{\mu}_n$ in Eq. (A1d) increases the energy of that moment, as expected for XY anisotropy. However, we find that the negative contribution of the h_x^{**} term can offset the former positive contribution, leading to a net decrease in the normalized average energy per moment

$$\frac{E_{ave}}{S^2J_2} = \frac{1}{n_\lambda}\sum_{n=1}^{n_\lambda}\frac{E_n}{S^2J_2}, \quad \text{(A20b)}$$

where n_λ is the integer number of moment layers per commensurate wavelength that is assumed for the in-plane helix.

In order to compare the value of $E_{ave}/(S^2J_2)$ with that calculated at $T = 0$ for an in-plane helix/fan for the same h_x^{**} [15], in Eq. (A20a), we set

$$J_{12} = -4\cos(kd) \quad \text{(A21a)}$$

according to Eq. (A14), where

$$kd = 2\pi m/n_\lambda \quad \text{(A21b)}$$

is the turn angle in Fig. 1 between adjacent layers of a helix in zero applied field with integer $m < n_\lambda$, and is assumed to be independent of both the applied and anisotropy fields. For this comparison, we also set

$$J_{02} = 0. \quad \text{(A22)}$$

[1] D. C. Johnston, Magnetic Susceptibility of Collinear and Noncollinear Heisenberg Antiferromagnets, Phys. Rev. Lett. **109**, 077201 (2012).

[2] D. C. Johnston, Unified molecular field theory for collinear and noncollinear Heisenberg antiferromagnets, Phys. Rev. B **91**, 064427 (2015).

[3] For extensive comparisons of the unified MFT with experimental data, see D. C. Johnston, Unified molecular field theory for collinear and noncollinear Heisenberg antiferromagnets, arXiv:1407.6353v1.

[4] D. C. Johnston, Magnetic dipole interactions in crystals, Phys. Rev. B **93**, 014421 (2016).

[5] D. C. Johnston, Influence of uniaxial single-ion anisotropy on the magnetic and thermal properties of Heisenberg antiferromagnets within unified molecular field theory, Phys. Rev. B **95**, 094421 (2017).

[6] D. C. Johnston, Influence of classical anisotropy fields on the properties of Heisenberg antiferromagnets within unified molecular field theory, Phys. Rev. B **96**, 224428 (2017).

[7] A. Yoshimori, A New Type of Antiferromagnetic Structure in the Rutile Type Crystal, J. Phys. Soc. Jpn. **14**, 807 (1959).

[8] P. A. Herpin and P. Meriel, Étude de L'Antiferromagnétisme helicoidal de $MnAu_2$ par diffraction de neutrons, J. Phys. Radium **22**, 337 (1961).

[9] M. Reehuis, W. Jeitschko, M. H. Möller, and P. J. Brown, A neutron diffraction study of the magnetic structure of $EuCo_2P_2$, J. Phys. Chem. Solids **53**, 687 (1992).

[10] V. Basso, E. Ferraro, and M. Piazzi, Thermodynamic transport theory of spin waves in ferromagnetic insulators, Phys. Rev. B **94**, 144422 (2016).

[11] X. Tan, G. Fabbris, D. Haskel, A. A. Yaroslavtsev, H. Cao, C. M. Thompson, K. Kovnir, A. P. Menushenkov, R. V. Chernikov, V. O. Garlea, and M. Shatruk, A transition from localized to strongly correlated electron behavior and mixed valence driven by physical or chemical pressure in ACo_2As_2 (A = Eu and Ca), J. Am. Chem. Soc. **138**, 2724 (2016).

[12] N. S. Sangeetha, V. K. Anand, E. Cuerco-Reyes, V. Smetana, A.-V. Mudring, and D. C. Johnston, Enhanced moments of Eu in single crystals of the metallic helical antiferromagnet $EuCo_{2-y}As_2$, Phys. Rev. B **97**, 144403 (2018).

[13] J. Jensen and A. R. Mackintosh, *Rare Earth Magnetism* (Clarenden Press, Oxford, 1991).

[14] T. Nagamiya, K. Nagata, and Y. Kitano, Magnetization Process of a Screw Spin System, Prog. Theor. Phys. **27**, 1253 (1962).

[15] D. C. Johnston, Magnetic structure and magnetization of helical antiferromagnets in high magnetic fields perpendicular to the helix axis at zero temperature, Phys. Rev. B **96**, 104405 (2017); **98**, 099903(E) (2018).

[16] Y. Kitano and T. Nagamiya, Magnetization Process of a Screw Spin System. II, Prog. Theor. Phys. **31**, 1 (1964).

[17] T. Nagamiya, Helical Spin Ordering—1 Theory of Helical Spin Configurations, Solid State Phys. **20**, 305 (1967).

[18] J. M. Robinson and P. Erdös, Behavior of Helical Spin Structures in Applied Magnetic Fields, Phys. Rev. B **2**, 2642 (1970).

[19] See Supplemental Material at http://link.aps.org/supplemental/10.1103/PhysRevB.99.214438 for additional plots of data generated using the theory in the main text and in the Appendix.